J. Fluid Mech. (2012), *vol.* 693, *pp.* 345–366. © Cambridge University Press 2012
doi:10.1017/jfm.2011.535

Suspensions with a tunable effective viscosity: a numerical study

L. Jibuti, S. Rafaï and P. Peyla†

Laboratoire Interdisciplinaire de Physique – Université Joseph Fourier, Grenoble 1 – CNRS, BP87, F-38402 Saint Martin d'Hères, France

(Received 31 March 2011; revised 15 November 2011; accepted 2 December 2011; first published online 12 January 2012)

In this paper, we conduct a numerical investigation of sheared suspensions of non-colloidal spherical particles on which a torque is applied. Particles are mono-dispersed and neutrally buoyant. Since the torque modifies particle rotation, we show that it can indeed strongly change the effective viscosity of semi-dilute or even more concentrated suspensions. We perform our calculations up to a volume fraction of 28 %. And we compare our results to data obtained at 40 % by Yeo and Maxey (*Phys. Rev.* E, vol. 81, 2010, p. 62501) with a totally different numerical method. Depending on the torque orientation, one can increase (decrease) the rotation of the particles. This results in a strong enhancement (reduction) of the effective shear viscosity of the suspension. We construct a dimensionless number Θ which represents the average relative angular velocity of the particles divided by the vorticity of the fluid generated by the shear flow. We show that the contribution of the particles to the effective viscosity can be suppressed for a given and unique value of Θ independently of the volume fraction. In addition, we obtain a universal behaviour (i.e. independent of the volume fraction) when we plot the relative effective viscosity divided by the relative effective viscosity without torque as a function of Θ. Finally, we show that a modified Faxén law can be equivalently established for large concentrations.

Key words: low-Reynolds-number flows, rheology, suspensions

1. Introduction

Solid particles suspended in a conventional Newtonian liquid form a suspension. This composite fluid constitutes a widespread fluid material in nature as well as in industry (Russel, Saville & Schowalter 1989). Fluids with controllable viscosity when an external field is applied are of considerable interest because of their occurrence in many kinds of industrial devices such as active dampers, clutches or brakes (Lim, Park & Kim 2005; Phani & Venkatraman 2005; Tan, Stanway & Bullough 2006). For example, with regard to automobile dampers: depending on road conditions, the viscosity of the damping fluid needs to be adjusted. An external field is used to modify the fluid properties by exerting a torque on suspended particles of nanometric or micrometric size. In electro-rheological (ER) fluids (Marshall, Zukovski & Goodwin 1989; Lemaire *et al.* 2008), polarizable particles are dispersed in a non-conducting liquid. When the suspension is submitted to an electric field, each dipolar particle can

† Email address for correspondence: Philippe.Peyla@ujf-grenoble.fr

https://doi.org/10.1017/jfm.2011.535 Published online by Cambridge University Press

align itself along the direction of the electric field. In some ER fluids, a rotation of the particles can be induced by the electric field. This rotation as well as its impact on the effective viscosity of the overall suspension has been experimentally observed (Lemaire *et al.* 2008). This phenomenon can be used to tune the effective viscosity of a suspension. Another observed phenomenon is clustering: the particles group together in elongated aggregates due to their attractive dipole–dipole interaction of magnetic or electrical origin. These two effects reversibly change the mechanical properties and thus the rheology of the medium. The possibility of changing the viscosity of a suspension by exerting a torque on its particles has also been demonstrated on ferrofluids subjected to a rotating magnetic field (Bacri *et al.* 1995). Ferrofluids are suspensions of rigid particles possessing a magnetic dipole. By applying a time-varying external magnetic field, a torque is exerted on particles, which thus rotate. This kind of effect exists not only for industrial applications but also for biological suspensions where the gravitational field is suspected to exert a torque on inhomogeneous spherical unicellular algae (Ishikawa & Pedley 2007; Rafaï, Jibuti & Peyla 2010). By changing cells rotation in a shear flow, gravity might impact flow properties of algae suspensions.

Brenner (1970) analytically studied the dynamics of polar spherical particles in a shear flow. The suspension is submitted to an external field which modifies the rotation of the spheres and therefore the effective viscosity of the suspension. This work was inspired by an experimental study (Rosensweig, Kaiser & Miskolczy 1969) on magnetic fluids. In the dilute regime, where hydrodynamic interactions can be neglected, the case of dipolar spherical particles in an external field can be solved analytically (see below).

For higher concentrations, numerical investigations are necessary. We refer here to the work of Prosperetti and his group (Marchioro, Tanksley & Prosperetti 2000; Marchioro *et al.* 2001; Wang & Prosperetti 2001; Ichiki & Prosperetti 2004), hereafter referred to collectively as Prosperetti *et al.* They used a direct simulation method and studied the behaviour of a suspension subjected to a torque in a statistically non-uniform flow and the behaviour of a suspension subjected to a uniform shear flow. Feng *et al.* (2006) used a boundary element method and studied a set of force-free translationally mobile spheres confined between a pair of no-slip parallel plates. The spheres rotate at an imposed position-independent angular velocity ω_z by applying a given torque. There is no imposed shear rate: the rotation of the spheres generate a suspension-scale simple shear (Couette) flow. Feng *et al.* (2006) also used a Poiseuille geometry. Yeo & Maxey (2010) used a force-coupling method to study sheared suspensions for high concentrations and submitted to a torque. For concentration higher than 48 %, they observe a regular and periodic arrangement of the particles in the flow. Below that value, including 40 %, they observe a homogeneous sheared suspension without any rearrangement.

In this paper, we use the fluid particle dynamics method (Tanaka & Araki 2000) to investigate the effect of torque on the rheology of a suspension of spherical particles. We analyse the competition between an imposed shear flow and an applied torque, as well as their respective contribution to the total effective viscosity on a range of volume fraction from 0 to 28 %. We obtain a universal behaviour independent of the volume fraction when we plot the total relative effective viscosity divided by the total relative effective viscosity in the absence of torque as a function of the dimensionless

https://doi.org/10.1017/jfm.2011.535 Published online by Cambridge University Press

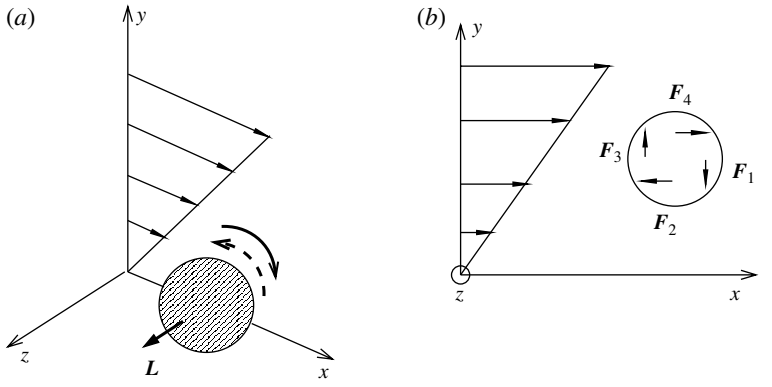


FIGURE 1. (*a*) Particle in a shear flow submitted to an external torque $\boldsymbol{L}$. The flow makes the particle rotate in one direction (solid arrow) while the torque induces a rotation in the same direction or in the opposite direction (dashed arrow) depending on the orientation of $\boldsymbol{L}$. (*b*) In our simulations, the torque is applied with a set of tangential forces $\boldsymbol{F}_i$ with $i = 1, \ldots, 4$ applied to each sphere in the xOy plane.

number Θ:

$$\Theta = \frac{\dot{\gamma}/2 + \langle \omega_z \rangle}{\dot{\gamma}/2}. \tag{1.1}$$

It represents the difference between the angular rotation of the particles $\langle \omega_z \rangle$ and the solid rotation component of the sheared fluid ($\dot{\gamma}/2$) in the absence of particles, divided by $\dot{\gamma}/2$. In the absence of an external torque, the particles' angular rotation is equal to $-\dot{\gamma}/2$ and $\Theta = 0$. This number can be either positive or negative depending on whether the torque orientation is anti-parallel or parallel to the flow vorticity (figure 1). Θ is the dimensionless number used throughout this paper. The symbol $\langle . \rangle$ means that we average on the set of particles. Since we impose a constant torque on each particle, we average the angular velocity on the set of particles. Note that Θ is meaningful only when $\dot{\gamma}$ is non-zero.

We perform simulations up to 28 % and we also include the plot of Yeo & Maxey (2010) (data obtained at 40 % with a different numerical method). We show that they are perfectly consistent with our results when these data are plotted as a function of Θ.

The volume fraction ϕ is defined as the volume of the set of particles divided by the total volume of the suspension. On each particle, the same value of the torque is applied. When the externally applied torque is anti-parallel to the vorticity (z-axis in figure 1), the torque slows down particle rotation and the effective viscosity is increased. This can be understood since particles create a counter-rotating flow opposed to that of the shear flow. Therefore, in order to impose the same value of the shear rate $\dot{\gamma}$, the shear stress σ_{xy} must be larger. Thus, the effective viscosity which can be expressed as $\eta_{eff} = \sigma_{xy}/\dot{\gamma}$ is increased. On the contrary, when the particle rotation is enhanced by an external torque parallel to the vorticity, it is easier to shear the suspension and η_{eff} decreases.

We show that formation of aggregates of particles is not necessary to obtain a strong modification of the effective viscosity: the modification of particle rotation is indeed sufficient to create a shear thinning or shear thickening effect. Faxén's second law (Happel & Brenner 1983), which is a relationship between applied torque and the

https://doi.org/10.1017/jfm.2011.535 Published online by Cambridge University Press

rotation velocity of particles, is usually valid for dilute suspensions. Here, we derive an empirical form of Faxén's second law valid from dilute to concentrated suspensions (up to 40 %).

In § 2, we briefly present the well-known results concerning the effective viscosity of sheared suspensions. In § 3, we apply a torque on particles in a dilute suspension under shear. We analytically derive the effective viscosity as a function of Θ. In § 4, we explain the details of our numerical method, fluid particle dynamics (FPD). We compare some results concerning canonical examples such as a Stokes flow past a sphere, a sphere in a shear flow with and without an applied torque. In order to test how the contact between particles is handled by the FPD method, we perform and analyse two sphere collisions. In § 5, we use the FPD method to simulate a suspension of spherical particles. We first apply a constant torque on each sphere in a fluid at rest (in the absence of a shear flow). We compare our results on vortex viscosity with those of Prosperetti *et al.* as well as Feng *et al.* (2006). We also compare our numerical results on shear viscosity in the absence of torque with other published results. Then, returning to our work (rotating particles submitted to a torque and a shear flow), we show that plotting the effective viscosity as a function of Θ reveals a universal behaviour (i.e. independent of the volume fraction). Finally, we conclude in § 6.

2. Effective viscosity of suspensions of torque-free and rigid particles

It is well known that the effective viscosity η^0_{eff} of a sheared suspension of torque-free spherical particles follows a virial expansion (Russel *et al.* 1989):

$$\eta^0_{eff} = \eta[1 + \alpha\phi + \beta\phi^2 + O(\phi^3)], \tag{2.1}$$

where ϕ is the volume fraction defined as the volume of particles normalized by the total volume of the suspension, η being the viscosity of the suspending Newtonian fluid. For a suspension of hard spheres, the linear term (the intrinsic viscosity) is $\alpha = 2.5$, as calculated by Einstein (1906, 1911) for a strong dilution. Then, when the semi-dilute regime is reached (for $\phi > 2\,\%$), the particles get closer and start to interact hydrodynamically. Batchelor & Green (1972) showed that hydrodynamic interactions contribute to the second order in ϕ. They found $\beta = 5.2 \pm 0.3$ for a non-Brownian suspension where particles are uniformly distributed. A more precise estimate of $\beta = 5.0$ has been achieved by Cichocki & Felderhof (1988). For more concentrated suspensions, interactions with three or even more bodies contribute to the effective viscosity, and the empirical law of Krieger & Dougherty (1959) describes η^0_{eff} for a broad range of volume fractions:

$$\eta^0_{eff} = \frac{\eta}{(1 - \phi/\phi_m)^{\alpha\phi_m}}, \tag{2.2}$$

where ϕ_m corresponds to the maximum random packing value of the volume fraction, and $\phi_m \approx 0.62$ for spherical and rigid particles. Note that (2.1) is the Taylor expansion up to order two of (2.2) for $\phi \ll 1$.

We define the relative effective viscosity in the absence of torque:

$$\Delta\eta^0_{eff} = \frac{\eta^0_{eff} - \eta}{\eta}. \tag{2.3}$$

https://doi.org/10.1017/jfm.2011.535 Published online by Cambridge University Press

3. Dilute suspensions in the presence of an external torque

Let us show how to calculate the contribution of an external torque exerted on each particle to the effective viscosity of a sheared suspension in the dilute regime. If we consider a dilute regime where spherical and neutrally buoyant particles of radius R are sufficiently far apart not to interact, we can consider a set of N independent particles like the one represented in figure 1. In the dilute regime and in the absence of an external torque, each particle rotates in the shear flow at the angular velocity $\boldsymbol{\omega}$ with the non-zero component $\omega_z = -\dot{\gamma}/2$. When an external torque $\boldsymbol{L}$ is applied to the particle along the z-axis, ω_z can be increased or decreased depending on the orientation of the torque. The total deviatoric stress σ_{xy}, which must be applied to the suspension in order to maintain a given shear rate $\dot{\gamma}$, is such that $\sigma_{xy} = \sigma^0_{xy} + \sigma^R_{xy}$, where σ^R_{xy} is the contribution of the external torque to the stress, and σ^0_{xy} is the deviatoric stress in the absence of torque. Batchelor (1970) showed that $\sigma^R_{xy} = N\,L/2\mathscr{V}$, where L is the component of the torque $\boldsymbol{L}$ along the z-axis, N is the number of particles and $\mathscr{V}$ is the total volume of the suspension. Since we are dealing with low-Reynolds-number hydrodynamics, we can use the linearity of the Stokes equation, which rules the incompressible fluid flow around particles. Faxén's second law (Happel & Brenner 1983) relates the external torque $\boldsymbol{L}$ exerted on the particle to the angular velocity $\boldsymbol{\omega}$:

$$\boldsymbol{L} = -8\pi R^3 \eta(\tfrac{1}{2}\,\boldsymbol{rot}\,\boldsymbol{V_0} - \boldsymbol{\omega}), \tag{3.1}$$

where $\boldsymbol{V_0}$ is the velocity field in the absence of particles; in our case, $\boldsymbol{V_0} = (\dot{\gamma}y, 0, 0)$. It gives $L = 8\pi R^3 \eta \Omega$, where $\Omega = \dot{\gamma}/2 + \omega_z$ represents the difference of angular velocity between ω_z and the one imposed by the shear flow alone, i.e. $-\dot{\gamma}/2$. For a torque-free particle, we have $\Omega = 0$ (i.e. $\omega_z = -\dot{\gamma}/2$). By using the definition of the volume fraction $\phi = N\,(4/3)\,\pi R^3/\mathscr{V}$, we obtain $L = 6\mathscr{V}/N\,\phi\eta\Omega$, which gives $\sigma^R_{xy} = 3\phi\eta\Omega$, and the contribution of the particles' relative rotation to the effective viscosity in the dilute regime, $\eta^R_{eff} = \sigma^R_{xy}/\dot{\gamma}$, is such that

$$\eta^R_{eff} = 3/2\phi\eta\Theta, \tag{3.2}$$

with $\Theta = \Omega/(\dot{\gamma}/2)$ as defined before. Note that η^R_{eff} has also been called 'vortex viscosity' by Condiff & Dahler (1964).

The total effective viscosity is given by $\eta_{eff} = (\sigma^0_{xy} + \sigma^R_{xy})/\dot{\gamma}$, and it leads to $\eta_{eff} = \eta^0_{eff} + \eta^R_{eff}$. As in (2.3), we can define the relative effective viscosity in the presence of torque, $\Delta\eta_{eff} = (\eta_{eff} - \eta)/\eta$, which for dilute suspensions gives

$$\Delta\eta_{eff}(\phi, \Theta) = \tfrac{5}{2}\,\phi(1 + \tfrac{3}{5}\Theta). \tag{3.3}$$

For example, when the external torque stops the particle rotation ($\omega_z = 0$ and $\Theta = 1$), one obtains $\Delta\eta_{eff} = 4\phi$. This gives a modified intrinsic viscosity such that $\alpha(\Theta = 1) = 4$, a result that was first derived by Brenner (1970).

4. Model and three-dimensional numerical method

Suspended elements are monodisperse spheres of radius R. For large particles, the Brownian motion is not taken into account. Spheres are suspended in a Newtonian liquid of viscosity η sheared between two walls. The two walls located at $y = \pm w/2$ move at $v_x = \pm v_0$ respectively, so that the shear rate is $\dot{\gamma} = 2v_0/w$. No-slip conditions are used at the fluid–wall interfaces. In order to neglect the effect of walls, we choose $15 < w/R < 20$, i.e. $w \gg R$. It has been shown by Davit & Peyla (2008) and Peyla & Verdier (2011) that the effects of walls through hydrodynamics interactions are

https://doi.org/10.1017/jfm.2011.535 Published online by Cambridge University Press

negligible when $w/R \gtrsim 12$. As an initial condition, we distribute the spheres randomly and homogeneously (taking care to avoid any overlaps). The fluid equation of motion around the spheres takes the usual form:

$$\rho(\partial_t + \boldsymbol{v} \cdot \nabla)\boldsymbol{v} = \nabla \cdot \boldsymbol{\sigma} + \boldsymbol{F}, \tag{4.1}$$

with the incompressibility condition $\nabla \cdot \boldsymbol{v} = 0$, where $\boldsymbol{v}$ is the velocity field and ρ is the constant fluid density. External volume forces are represented by $\boldsymbol{F}$. Note that our code is able to handle small but finite Reynolds numbers. However, in this work, Reynolds number are $\sim 10^{-2}$, therefore inertial effects are indeed negligible. We deal with neutrally buoyant particles with a density ρ equal to the fluid density. The ij-component of the stress tensor is given by the Newtonian law:

$$\sigma_{ij} = -P\delta_{ij} + \eta[\partial_i v_j + \partial_j v_i], \tag{4.2}$$

where P is the pressure field. Usually, spheres are taken into account through moving boundary conditions, which are quite difficult to handle numerically. This problem will be circumvented as follows. We use the 'fluid particle dynamics' (FPD) method, originally developed by Tanaka & Araki (2000) in two dimensions and extended to three dimensions by one of the authors (Peyla 2007; Davit & Peyla 2008). This kind of method is also known as a 'penalty method', and a mathematical analysis of such methods has been done by Maury (2009). Note that other methods such as lattice Boltzmann methods (Kromkamp *et al.* 2006) or Stokesian dynamics (Brady *et al.* 1988) could be used as well. The advantage of FPD is to explicitly avoid tracking the particles and thus avoid applying boundary conditions on a moving boundary. In this method, particles are defined as high-viscosity regions (η_p), in comparison to that of the solvent (η). Therefore, the flow field is defined in the entire domain and not only outside the spheres. Thus, at each time step (4.1) is solved outside and inside the particles but with a viscosity field $\eta'(\boldsymbol{r})$. We briefly summarize the main points of the numerical method; details can be found in the literature (Tanaka & Araki 2000; Peyla 2007; Davit & Peyla 2008).

The presence of particle number n is accounted for via an auxiliary field

$$\varphi_n(\boldsymbol{r}) = \tfrac{1}{2}\{1 + \tanh[(a - |\boldsymbol{r} - \boldsymbol{r}_n|)/\zeta]\}, \tag{4.3}$$

where ζ represents the fluid–particle interface thickness and $\boldsymbol{r}_n$ is the off-lattice centre of particle n. Thus, the radius of a sphere is $R \approx a + \zeta$. We choose $2\delta \leqslant a \leqslant 4\delta$ depending on the simulations, and $\zeta = (1/2)\delta$ where δ is the mesh size. In other words, the difficulty of the sharp interface between each sphere and the fluid is circumvented by introducing a diffuse (albeit sufficiently abrupt) interface. Of course, we choose a small value for ζ in order to have a sufficiently abrupt interface. The idea then is to introduce a viscosity field such that

$$\eta'(\boldsymbol{r}) = \eta + (\eta_p - \eta)\sum_{n=1}^{N} \varphi_n(\boldsymbol{r}), \tag{4.4}$$

where N is the total number of spheres. This ensures that, sufficiently far from a particle, the local viscosity is $\eta' = \eta$ (the solvent viscosity), and inside the particle $\eta' = \eta_p$ (the particle viscosity). The viscosity contrast is fixed to $\eta_p/\eta = 100$. This choice is made to avoid any recirculation of the fluid inside the spheres, which can thus be considered as rigid (Tanaka & Araki 2000). The drop of the viscosity from one mesh to another is close to linear for $\zeta = 0.5\delta$ and starts to be nonlinear for higher

https://doi.org/10.1017/jfm.2011.535 Published online by Cambridge University Press

values of ζ. However, we show that the choice of $\zeta \leqslant \delta$ does not really influence our results (see figures 2, 3 and 4).

Equation (4.1) is solved on a MAC grid (Peyret & Taylor 1963), where the pressure field $P(\boldsymbol{r})$, the viscosity field $\eta(\boldsymbol{r})$, and the stress field are calculated at the centre of each cubic mesh i of size $\delta \times \delta \times \delta$ located in (x_i, y_i, z_i), while fluid velocity components are calculated at the centre of each face of the mesh. This ensures that each term involved in (4.1) is calculated at the same point of the mesh grid (Peyret & Taylor 1963). Note that our calculations are done for several volume fractions up to $\phi = 28\,\%$. This corresponds to $N \approx 530$ when $R \approx 3\delta$ or to $N \approx 230$ when $R \approx 5\delta$ in a simulation box of $60 \times 60 \times 60$ meshes. We conducted our simulations with various diameters in order to check that the choice of the diameter does not affect our results. For bigger ϕ-values, we cannot avoid effects such as the formation of depletion layers close to the walls (Davit & Peyla 2008).

In order to apply an external torque perpendicular to the shear plane (xOy) on the particles, tangential forces $\boldsymbol{F_i}$, where $i = 1, \ldots, 4$, are applied to each particle in the xOy plane (figure 1*b*). Each force has the same intensity. Then, the same torque $\boldsymbol{L} = \Sigma_{i=1}^{4} \boldsymbol{r_i} \times \boldsymbol{F_i}$ is applied to each particle. In order to change $\boldsymbol{L}$, we vary the components $\boldsymbol{F}_i$.

The numerical procedure is as follows. For each time step $\delta t = 0.001$, the pressure and velocity are calculated following a standard projection method, ensuring incompressibility of the fluid (Peyret & Taylor 1963). Depending on the simulation, values from $\dot{\gamma} = 10^{-5}/\delta t = 10^{-2}$ to $\dot{\gamma} = 10^{-6}/\delta t = 10^{-3}$ are used. Inertia is negligible in (4.1) since only small Reynolds numbers are considered here: $10^{-2} < Re = \rho \dot{\gamma} a^2/\eta < 10^{-1}$. The typical simulation box size is $\ell_x = \ell_y = \ell_z = w = 60\delta$. Here, $\delta = 1$. Boundary conditions are such that the fluid velocity is imposed on the upper ($y = +w/2$) and lower ($y = -w/2$) wall, $v_x(x, y = \pm w/2, z) = \pm v_0$, while periodic boundary conditions are adopted in the x and z directions. For each time step, the off-lattice centre $\boldsymbol{r}_n$ of particle n is moved as follows: $\boldsymbol{r}_n(t + \delta t) = \boldsymbol{r}_n(t) + \delta t\, \bar{\boldsymbol{v}}_n(t)$, where $\bar{\boldsymbol{v}}_n(t)$ is the fluid velocity averaged on the high-viscosity region surrounding the centre of the sphere n at time t. It ensures shape preservation of particles. The viscosity field is then reconstructed (Tanaka & Araki 2000) considering the new positions of the spheres at time $t + \delta t$. This gives rise to a new bulk viscosity field, which is substituted in (4.1), which is again solved for $t + \delta t$. The effective viscosity of the suspension is evaluated by calculating the tangential force per unit surface exerted by the walls on the fluid: $f_x^{\pm}(t) = \bar{\sigma}_{xy}(y = \pm w/2,\, t)\, n_y$, which is necessary to maintain a constant velocity $\pm v_0$ on the upper (+) and lower (−) walls. The unit vector $\boldsymbol{n}$ is normal to the fluid–wall interface, and $\bar{\sigma}_{xy}$ represents the average of $\sigma_{xy}(\pm w/2)$ on the whole surface of the fluid in contact with the walls. The time-dependent effective viscosity is thus $\eta_{eff}(t) = 1/2\,[f_x^{+}(t) - f_x^{-}(t)]/\dot{\gamma}$. Initially, we start with a random distribution of sphere positions. After a transient regime, the effective viscosity reaches a plateau and remains stable after several thousand time steps. By eliminating the initial transient regime and averaging the plateau values, we finally obtain the averaged effective viscosity $\bar{\eta}_{eff}$ calculated for a given initial configuration.

In order to calculate the correct value of the volume fraction $\phi = N\,(4/3)\,\pi R^3/\mathscr{V}$, the volume of the particles must be calculated carefully by taking into account the diffuse interface (of size ζ) of each particle. To determine the effective radius R of a particle, we consider Stokes flow past a sphere. We apply a force $\boldsymbol{f_0}$, which is necessary to compensate the drag force $6\pi\eta R\boldsymbol{V_0}$ exerted by the external flow (figure 2), $\boldsymbol{V_0}$ being the fluid velocity at infinity. For a given force $\boldsymbol{f_0}$, the sphere is immobile in the flow and we determine its effective radius R associated with the parameters

https://doi.org/10.1017/jfm.2011.535 Published online by Cambridge University Press

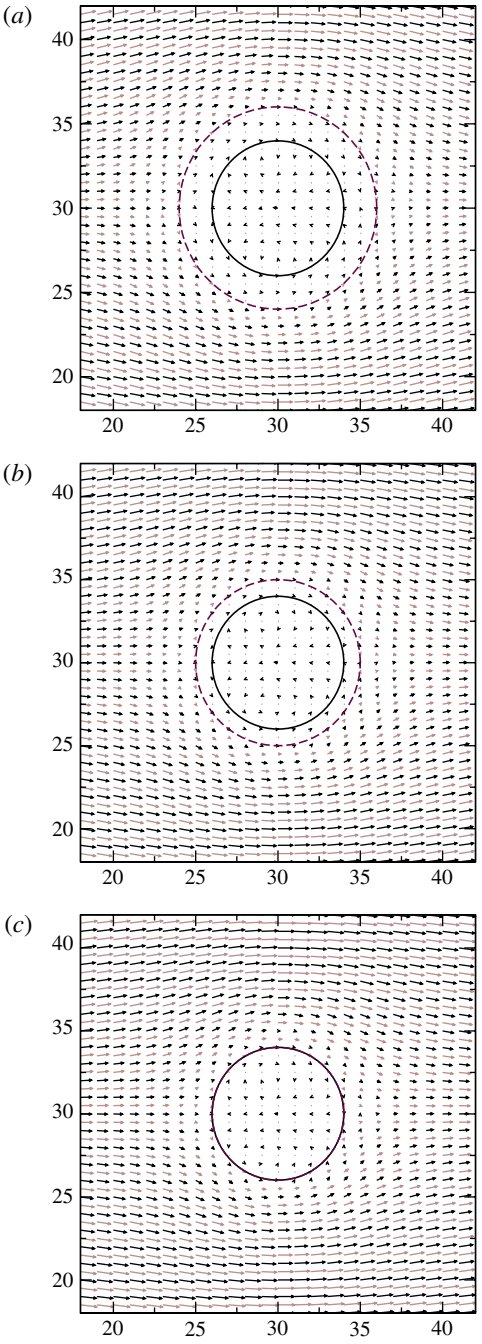


FIGURE 2. (Colour online available at journals.cambridge.org/flm) Stokes flow past a sphere with $a = 4\delta$. The black arrows represent the numerical results and the lighter arrows are calculated analytically (Landau & Lifschitz 1959). The two fields (numerical and analytical) are calculated on two $\delta/2$-shifted grids in order to be visually compared. The velocity is represented in the xy-plane that crosses the middle of the sphere. Three different values of ζ are used: (*a*) $\zeta = \delta$, (*b*) $\zeta = 0.5\delta$ and (*c*) $\zeta = 0$. The solid and dashed circles represent the radius a and $a + 2\zeta$ respectively. The size of the simulation box is $60\delta \times 60\delta \times 60\delta$.

https://doi.org/10.1017/jfm.2011.535 Published online by Cambridge University Press

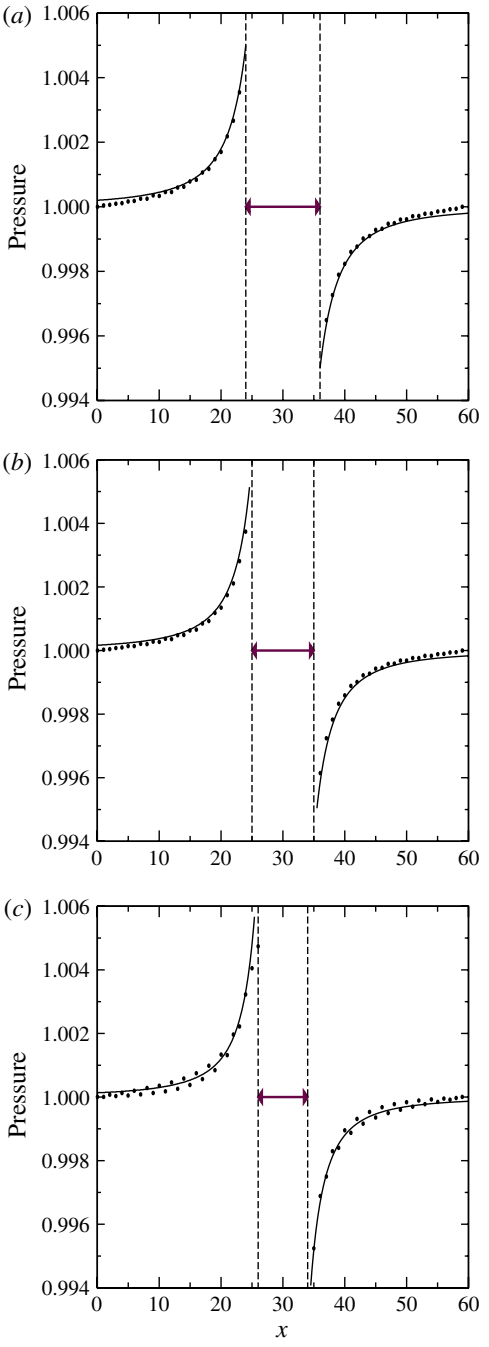


FIGURE 3. (Colour online) The pressure field along the x-axis for a Stokes flow past a sphere with $a = 4\delta$. The dots represent numerical points while the curve is the analytic value (Landau & Lifschitz 1959). Three different values of ζ are used: (*a*) $\zeta = \delta$, (*b*) $\zeta = 0.5\delta$ and (*c*) $\zeta = 0$. One can observe oscillations for the pressure field for $\zeta = 0$. The double arrow indicates the region occupied by the sphere along x. The size of the simulation box is $60\delta \times 60\delta \times 60\delta$.

https://doi.org/10.1017/jfm.2011.535 Published online by Cambridge University Press

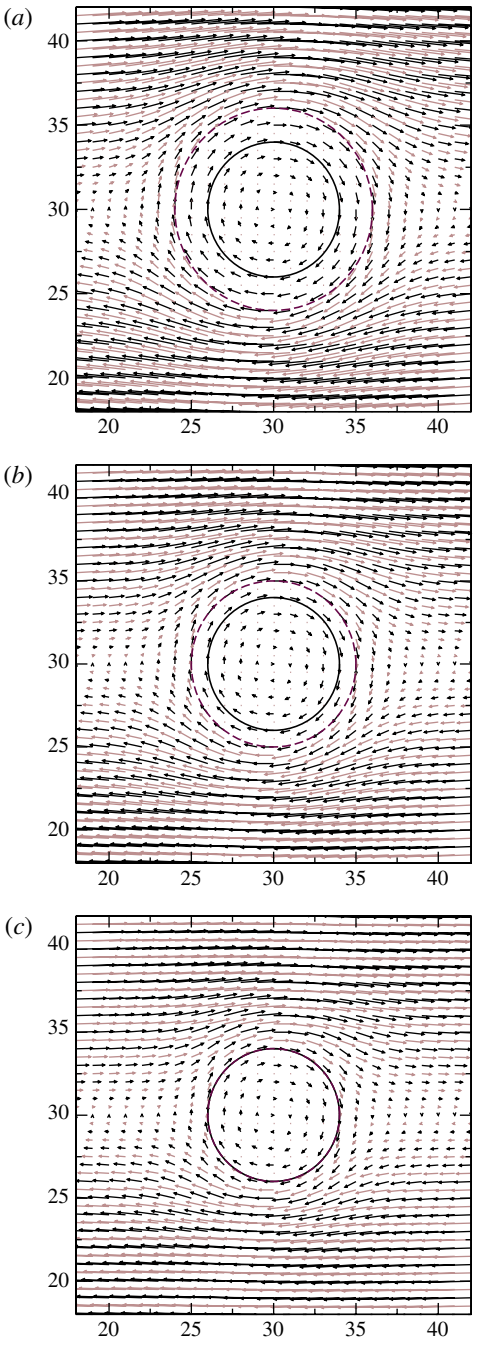


FIGURE 4. (Colour online) A sphere in a pure shear flow with $a = 4\delta$. The black arrows represent the numerical results and the lighter arrows are calculated analytically in (4.5). The two fields (numerical and analytical) are calculated on two $\delta/2$-shifted grids in order to be visually compared. The velocity is represented in the xy-plane that crosses the middle of the sphere, parallel to the shear plane. Three different values of ζ are used: (*a*) $\zeta = \delta$, (*b*) $\zeta = 0.5\delta$ and (*c*) $\zeta = 0$. The solid and dashed circles represent the radius a and $a + 2\zeta$ respectively. The size of the simulation box is $60\delta \times 60\delta \times 60\delta$.

https://doi.org/10.1017/jfm.2011.535 Published online by Cambridge University Press

a and ζ. It is found that the effective radius R remains close to $a+\zeta$ up to small values of a such as $a=2\delta$, with a precision of $\sim$1 %. Then, once R is obtained, it is straightforward to obtain the volume fraction ϕ.

The Stokes flow around the spheres is sufficient to avoid particle interpenetrations. In the literature, some authors (Tanaka & Araki 2000) have introduced short-range forces in order to avoid interpenetrations, whereas others (Maury 2006) have used a projection method on the velocity field to constrain particles not to interpenetrate. Here, we prefer not to introduce such methods, in order to avoid any numerical artifacts at high density. This is why we present simulations at volume fractions below $\phi=28\,\%$, where a very stable value of $\phi(t)$ is obtained (overlaps between particles would result in a variation, i.e. a decrease, of $\phi(t)$). Therefore, our simulations are sufficient for low volume fractions but are not appropriate at higher volume fractions (more than 28 %), where a short-range treatment, like those described above, should be introduced.

In order to explicitly show that lubrication forces between particles are fully resolved in our simulations (at least below $\phi=28\,\%$), two sphere collisions are simulated and analysed below. In order to show the reliability of our simulations, some tests have already been published (Tanaka & Araki 2000; Peyla 2007; Davit & Peyla 2008). Here, we compare our numerical results with analytical results for canonical cases: a Stokes flow past a sphere (figures 2, 3 and 5*a*), a sphere in a pure shear flow (figures 4 and 5*b*) with $\Theta=0$, and a sphere in a shear flow submitted to a torque (figure 6) (i.e. $\Theta=\pm1$). Regarding the last two examples, we compare our results with the following solution (Mikulencak & Morris 2004) for the velocity field:

$$\begin{cases} V_x=\dfrac{\dot\gamma}{2}\left\{y\left[1-\dfrac{R^5}{r^5}\right]+y\left[1-\dfrac{R^3}{r^3}\right]-5R^3x^2y\left[\dfrac{1}{r^5}-\dfrac{R^2}{r^7}\right]-\dfrac{(1-\Theta)R^3y}{r^3}\right\},\\ V_y=\dfrac{\dot\gamma}{2}\left\{x\left[1-\dfrac{R^5}{r^5}\right]-x\left[1-\dfrac{R^3}{r^3}\right]-5R^3xy^2\left[\dfrac{1}{r^5}-\dfrac{R^2}{r^7}\right]+\dfrac{(1-\Theta)R^3x}{r^3}\right\},\\ V_z=-\dfrac{5\dot\gamma}{2}xyzR^3\left[\dfrac{1}{r^5}-\dfrac{R^2}{r^7}\right] \end{cases} \quad (4.5)$$

with $r=\sqrt{x^2+y^2+z^2}$. We can clearly see very good agreement between the two velocity fields, which are plotted in the xy-plane cutting the sphere in half. In figures 4 and 6, the inner velocity field is simply the rigid rotation of the sphere. On the overall simulation box, an error smaller than 1 % is obtained for the numerical velocity field. Concerning the pressure field in a Stokes flow past a sphere (figure 3), we also compare the value of our numerical results with the pressure along the x-axis (Landau & Lifschitz 1959). Again, very good agreement is obtained. The velocity field and the pressure field are compared for several values of ζ (defined before). We can see that for small values of ζ (0, 0.5δ and δ) the agreement is quite good and the numerical results do not depend too much on ζ. However, we can see that for $\zeta=0$ some small oscillations appear in the numerical values of the pressure (figure 3). That is why we choose $\zeta=0.5\delta$ for all our simulations, which ensures the most reliable velocity and pressure fields combined with a sufficiently abrupt interface.

In figure 6, we show the velocity field around a single sphere for three different values of Θ: $\Theta=-1.0$ ($\omega_z=-\dot\gamma$), $\Theta=+1.0$ ($\omega_z=0$) and $\Theta=0$ ($\omega_z=-\dot\gamma/2$). The field flow is represented in the shear xy-plane. We compare our numerical results with the analytical velocity field (4.5). Here too an error smaller than 1 % is obtained when we compare our results with the analytical solution. Again, the agreement is very

https://doi.org/10.1017/jfm.2011.535 Published online by Cambridge University Press

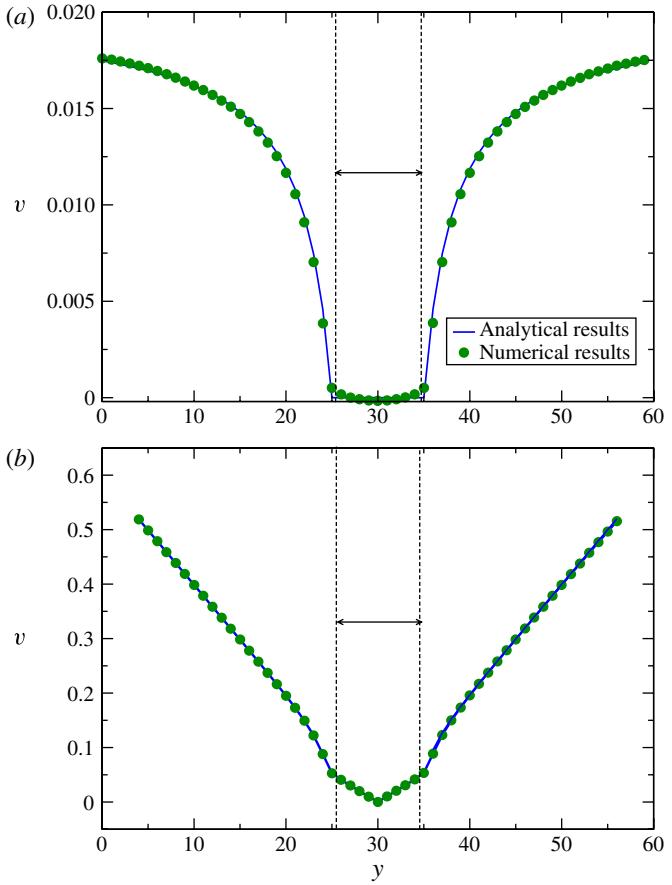


FIGURE 5. (Colour online) The velocity profiles $v = \sqrt{v_x^2 + v_y^2 + v_z^2}$ along the y-axis. The double arrow indicates the region occupied by the sphere along y. (a) For a Stokes flow past a sphere. The numerical results (circles) are compared to the analytical results (curve) (Landau & Lifschitz 1959) outside the sphere. (b) For a sphere in a pure shear flow. The numerical results (circles) are compared to the analytical results (curve) (4.5) outside the sphere.

good. In the next section we will include several spheres (up to around 500) in our simulations to work at different volume fractions.

Another good test of the method is the simulation of the collision between two spheres in a symmetrical shear flow xOy-plane. It allows us to test the contact events between two particles as well as the reversibility of the Stokes equation. In figure 7, we plot the trajectories $y(x)$ for different initial y interdistances; x and y are, respectively, the differences between the positions of the spheres along the x- and y-axes. The two spheres are initially moving toward each other, symmetrically positioned along the y-axis with respect to the line $v_x = 0$. The initial y interdistance between the particle centres is the impact parameter denoted by b. Of course, when they are very close, the two spheres are not in true physical contact at any time: a thin layer of fluid of thickness typically equal to ζ is clearly visible in figure 7 since the interdistance is slightly more than twice the radius R. Good agreement is obtained in the two cases $b/R = 1$ and $b/R = 0.6$ with the results of Da Cunha & Hinch (1996).

https://doi.org/10.1017/jfm.2011.535 Published online by Cambridge University Press

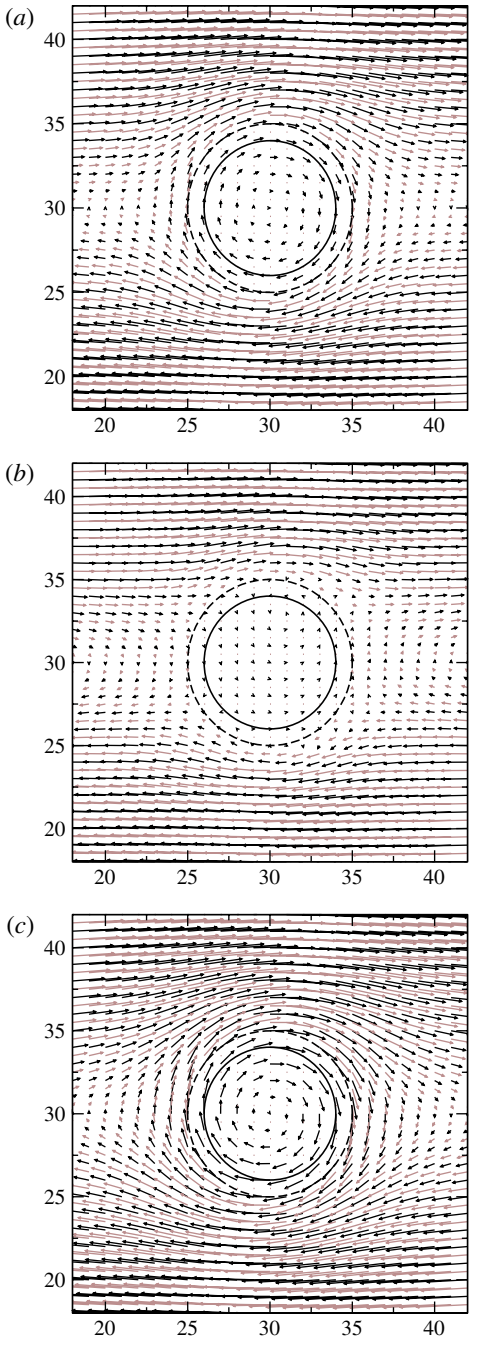


FIGURE 6. (Colour online) The velocity field around a single sphere of radius $R = 4\delta$ and $\zeta = 0.5\delta$ submitted to a torque in a pure shear flow. The black arrows represent the numerical results and the lighter arrows are calculated analytically. The two fields (numerical and analytical) are calculated on two $\delta/2$-shifted grids in order to be visually compared. The velocity is represented in the xy-plane that crosses the middle of the sphere and parallel to the shear plane. Three different values of Θ are used: (*a*) $\Theta = 0$, (*b*) $\Theta = +1$, and $\Theta = -1$. The solid and dashed circles represent the radius a and $a + 2\zeta$ respectively. The size of the simulation box is $60\delta \times 60\delta \times 60\delta$, much bigger than the sphere diameter.

https://doi.org/10.1017/jfm.2011.535 Published online by Cambridge University Press

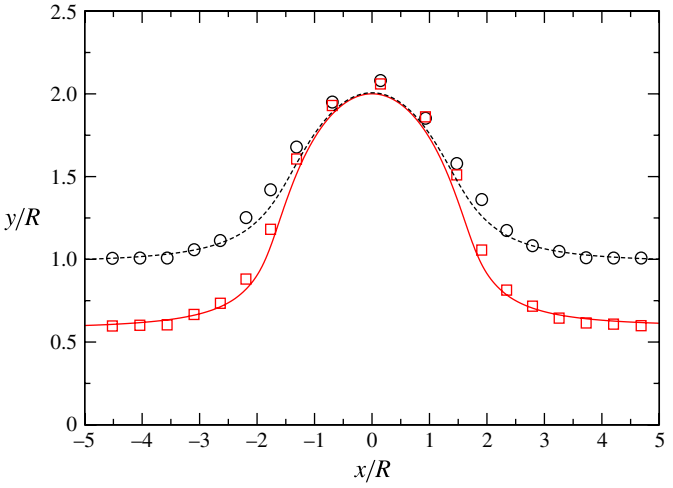


FIGURE 7. (Colour online) Particle trajectories of two identical and symmetrical spheres in a shear flow. The radius of each sphere is $R = 5\delta$ ($a = 4.5\delta$, $\zeta = 0.5\delta$). The circles ($b/R = 1$) and squares ($b/R = 0.6$) represent our numerical results. Here x and y represent the horizontal and vertical distance between the spheres respectively. The two curves represent the trajectories calculated from Da Cunha & Hinch (1996). Note the symmetrical shape of $y(x)$, which is due to the reversibility of the Stokes equation in the case of rigid spheres.

When the two spheres collide (if $b < 2R$), they form a doublet. This doublet rotates around the z-axis; its orientation is defined by the angle φ (figure 8). Initially, when the two spheres come into contact (at $\varphi = \varphi_0$, which depends on b), the doublet is rotating as a rigid system at a certain angular velocity. Then, for $\varphi = -\varphi_0$, the two spheres separate. Separation and contact, as well as the spheres' trajectories before and after $\varphi = 0$, are the mirror images of each other through the plane $x = 0$ (figure 7), simply reflecting the Stokes equation reversibility in the case of rigid spheres. The angular velocity of the doublet is not constant but increases to a maximum at $\varphi = 0$. Following the work of Bartok & Mason (1957), we compare the doublet rotation $[\varphi(t)]$ to the Jeffery orbit (Jeffery 1922) of an ellipsoid of revolution with an axis ratio of 2:

$$\tan(\varphi) = 2\tan\left(\frac{2\dot{\gamma}t}{5}\right). \tag{4.6}$$

Figure 8 shows excellent agreement between our numerical results, the law (4.6) and the experimental values of Bartok & Mason (1957). In this figure, time is conventionally fixed to $t = 0$ when the doublet is vertical (along the y-axis, i.e. $\varphi = 0$). These results show that lubrication forces between close spheres are indeed well resolved by our numerical method. However, as already mentioned, when the volume fraction is higher than 28 %, we cannot avoid some overlaps. Therefore, we restrict ourselves here to results below 28 %.

Note also that in our simulations we have not included dipole–dipole attractions (such as magnetic dipole interactions), since we would like to study the effect of the rotation of particles on the rheology separately from the clustering effects.

https://doi.org/10.1017/jfm.2011.535 Published online by Cambridge University Press

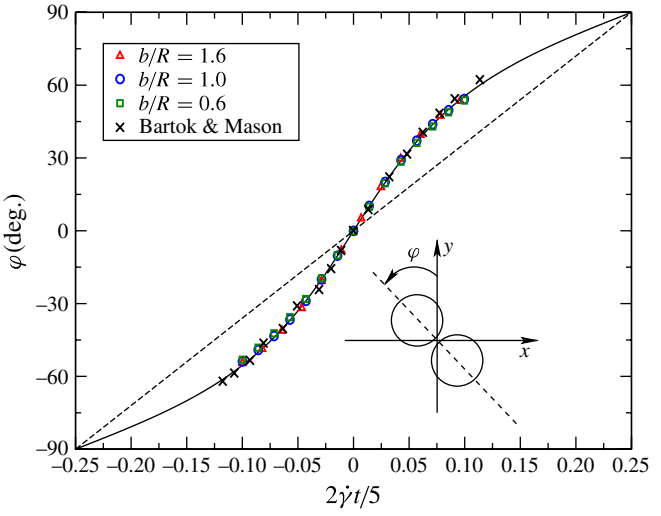


FIGURE 8. (Colour online) The variation of φ with time for different impact parameters and compared to (4.6) as well as experimental results of Bartok & Mason (1957).

5. Results

Feng *et al.* (2006) have calculated the contribution of torque applied to suspended particles in a fluid at rest to the effective viscosity $\eta^R_{eff}(\phi)$ (vortex viscosity). In order to compare our results with Feng *et al.* (2006) and Prosperetti *et al.* we apply the same torque L on each particle, and by averaging the angular velocity of the particles $\langle\omega_z\rangle$ (a value that depends on ϕ) we can easily obtain the vortex viscosity by using the following relation (Condiff & Dahler 1964; Feng *et al.* 2006):

$$\boldsymbol{\mathcal{L}} = 4\eta^R_{eff}(\phi)[\tfrac{1}{2}\boldsymbol{\nabla}\times\boldsymbol{V_0} - \langle\boldsymbol{\omega}\rangle], \tag{5.1}$$

where $\boldsymbol{\mathcal{L}} = N\boldsymbol{L}/\mathscr{V}$ is the total torque per unit volume. Note that this expression is an *a priori* constitutive law which applies to the suspension itself. It is different from Faxén's second law (3.1), which applies to a single sphere in a fluid. Equation (5.1) simply shows that the difference between the particles' angular velocity and the vorticity of the fluid is proportional to $\boldsymbol{\mathcal{L}}$. The coefficient of proportionality is the effective vortex viscosity. This expression, originally introduced by Condiff & Dahler (1964), has been *a posteriori* verified by Feng *et al.* (2006) in two different geometries. In our case, we apply the same torque $\boldsymbol{L}$ on each particle along the z-axis ($L > 0$) and the particles have a clockwise rotation. Following Batchelor (1970), $\mathscr{L} = 2\sigma^R_{xy}$, and thus by using (5.1), with $V_0 = 0$ (since the fluid is at rest when no torque is applied), and taking the z-component of $\boldsymbol{\omega}$, we obtain

$$\eta^R_{eff}(\phi) = \frac{\sigma^R_{xy}}{2\langle\omega_z\rangle}. \tag{5.2}$$

Here, the configuration (rotating particles in a fluid at rest) is a bit different from the other configuration studied in this paper (rotating particles in an imposed shear flow). In the first case, the value of the induced shear rate $\dot{\gamma}_{ind}$ depends on ϕ. Therefore, the corresponding value of Θ also depends on ϕ. However, by using (3.1) which holds for the dilute regime ($\phi \ll 1$), we obtain $\sigma_{xy} = N/(2V)8\pi\eta R^3\omega_z$. Thus $\eta^R_{eff}/\eta = 3/2\phi$ (Brenner 1970), equivalent to $\Theta = 1$ for a dilute suspension of non-rotating spherical

https://doi.org/10.1017/jfm.2011.535 Published online by Cambridge University Press

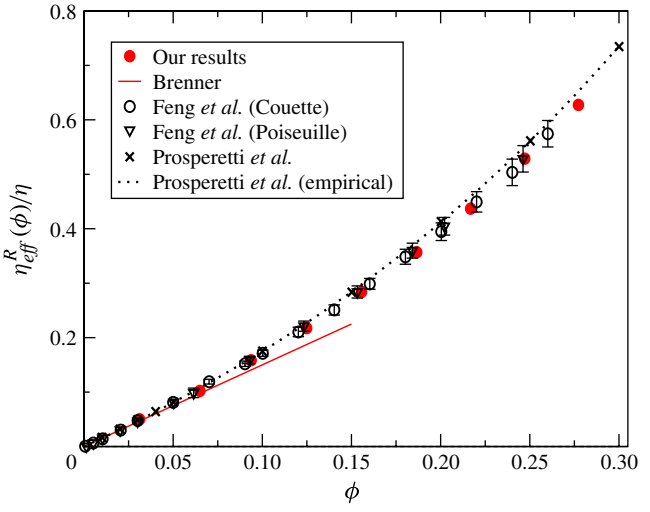


FIGURE 9. (Colour online) The vortex viscosity as a function of the volume fraction. The fluid is sheared by the identical rotation of the particles. In our simulations, the same torque is applied to each spherical particle.

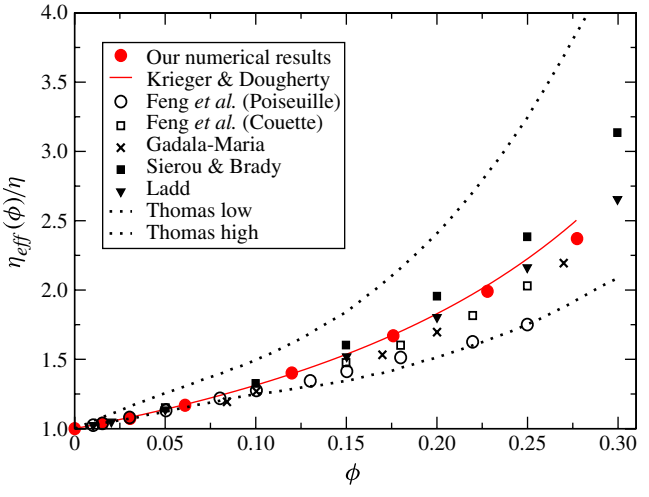


FIGURE 10. (Colour online) The effective shear viscosity as a function of the volume fraction when no torque is applied (i.e. $\Theta = 0$). Comparison is made with experimental data (upper and lower limits are given by Thomas 1969) as well as with the simulation results of others.

particles in an imposed shear flow. In figure 9, we compare our results to Feng's results and to the results obtained previously by Prosperetti *et al.* (the numerical results and the empirical law, $\eta^R_{eff}/\eta = 1.5\phi\ (1-\phi)^{1.5-0.41\phi}$). The agreement is indeed very good. As expected, at low ϕ the result of Brenner (1970) is recovered.

We can also calculate the effective viscosity when no torque is applied on a sheared suspension ($\dot{\gamma}$ imposed and $L = 0$), i.e. $\Theta = 0$. In the first case, the effective viscosity of the sheared suspension behaves like (2.2). In figure 10, we have plotted our

https://doi.org/10.1017/jfm.2011.535 Published online by Cambridge University Press

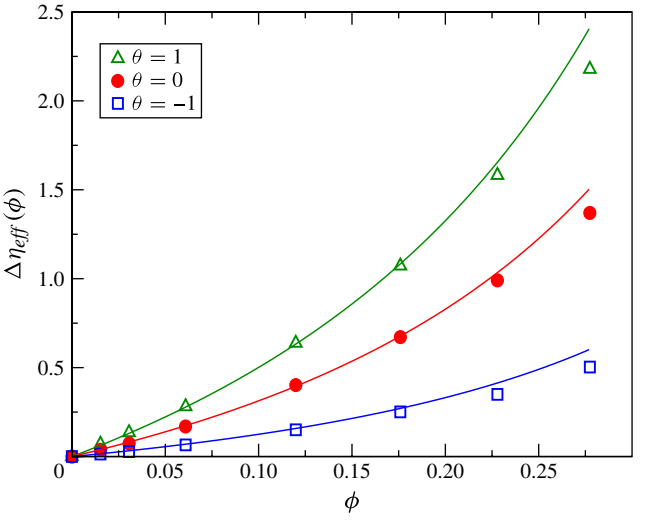


FIGURE 11. (Colour online) The relative effective viscosity as a function of the volume fraction ϕ for three different values of θ. The solid lines are calculated with (5.3).

numerical results as well as the results obtained previously (Thomas 1969; Gadala-Maria 1979; Ladd 1990; Sierou & Brady 2002; Feng *et al.* 2006). Here too we obtain very good agreement.

Now we focus on a sheared suspension in the presence of torque on each particle ($\dot{\gamma} \neq 0$, i.e. Θ finite) which represents our new results. We examine the competition between the torque exerted on each particle and the shear rate imposed by the flow. The torque can help to increase or decrease the rotation velocity of the particles in comparison to the rotation velocity ($\omega_z = -\dot{\gamma}/2$) imposed by the shear rate. This has already been examined for very dense suspensions by Yeo & Maxey (2010), who observed periodic arrangements for $\phi \geqslant 48\,\%$. Here, we examine the range of $0 < \phi < 28\,\%$. Still, we show in figure 12 that the results of Yeo and Maxey obtained for $\phi = 40\,\%$ (below concentration where arrangements are observed) are consistent with our results once plotted as a function of Θ (they are plotted as a function of a dimensionless torque by Yeo & Maxey 2010).

In figure 11, the relative effective viscosity is plotted for three values of Θ as a function of ϕ. When no torque is applied ($\Theta = 0$), we recover the nonlinear dependence of $\Delta\eta^0_{eff}$ well fitted by (2.2). When the particle rotation is stopped ($\Theta = 1$) the effective viscosity is increased, whereas it is decreased when particle rotation is in the same direction as that imposed by the shear flow ($\Theta = -1$). At $\phi = 28\,\%$, we see a small difference between Krieger and Dougherty's law and our data. This is due to a slight depletion of particles close to the walls, which occurs at a sufficiently high concentration; as shown in Davit & Peyla (2008), this tends to decrease the shear effective viscosity.

As predicted by (3.3) for dilute regimes, plotting the relative effective viscosity $\Delta\eta_{eff}$ as a function of Θ gives a set of linear curves which cross the zero viscosity axis for the same value $\Theta \approx -1.6 \pm 0.1$, close to $\Theta = -5/3$, and with a slope $3/2\phi$ (figure 12). But $\Delta\eta_{eff}$ is still linear for higher volume fractions up to 28 %, following the empirical law

$$\Delta\eta_{eff}(\phi, \Theta) = \Delta\eta^0_{eff}(\phi)(1 + \tfrac{3}{5}\Theta), \tag{5.3}$$

https://doi.org/10.1017/jfm.2011.535 Published online by Cambridge University Press

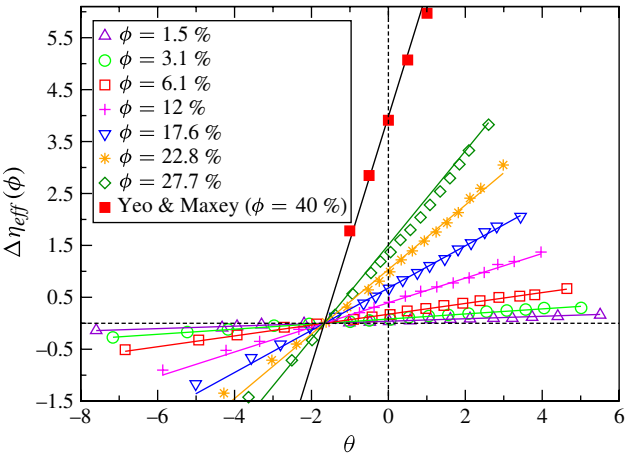


FIGURE 12. (Colour online) The relative effective viscosity as a function of Θ for different values of the volume fraction. The solid lines are obtained with (5.3). The Yeo & Maxey (2010) data are very well fitted by the law (5.3).

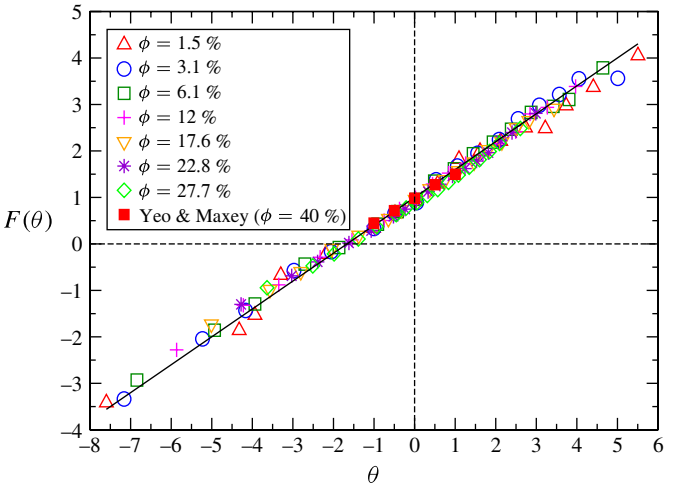


FIGURE 13. (Colour online) The ratio $F(\Theta)$ of the relative effective viscosities $\Delta\eta_{eff}$ and $\Delta\eta^0_{eff}$ as a function of Θ for different values of the volume fraction ϕ. A single master curve is obtained: $F(\phi, \Theta) = 1 + 3/5\Theta$ as predicted by (5.4) represented by the straight line. The Yeo & Maxey (2010) data are very well fitted by the law (5.4).

which tends to (3.3) when $\phi \ll 1$ since $\Delta\eta^0_{eff}$ tends to $5/2\phi$. Here the value of Θ is averaged on the N particles: $\Theta = \langle\Omega\rangle/(\dot{\gamma}/2) = 1 + \langle\omega_z\rangle/(\dot{\gamma}/2)$, where $\langle.\rangle$ denotes the average over the set of particles. Equation (5.3) fits our numerical results remarkably well, as shown in figures 11 and 12. The data points of Yeo & Maxey (2010), obtained for $\phi = 40\,\%$ using a totally different numerical method, are also very well fitted when represented as a function of Θ (see below). As is shown in figure 13, all the curves, whatever the value of ϕ, collapse on one single curve while plotting

https://doi.org/10.1017/jfm.2011.535 Published online by Cambridge University Press

$F(\Theta) = \Delta\eta_{eff}/\Delta\eta^0_{eff}$ as a function of Θ:

$$F(\Theta) = 1 + \tfrac{3}{5}\Theta. \tag{5.4}$$

Note that it is possible to obtain a negative relative effective viscosity for sufficiently high absolute values of Θ (for $\Theta < 0$). This is due to the rotation of particles (for $\Theta < 0$), which increases the shear rate, while a negative stress σ_{xy} has to be imposed to maintain the same value of $\dot\gamma$. Note that whatever the volume fraction, for the same value of $\Theta = -5/3$ (i.e. $\langle\omega_z\rangle = -4/3\dot\gamma$), the contribution of the particles to the effective viscosity can be suppressed by applying a critical torque L_c derived below.

We can also derive the expression of L from an empirically modified form of Faxén's second law. By transposing the expression of $L(\omega_z)$, i.e. (3.1), in the dilute regime to a concentrated regime, one can write

$$L = -\frac{12\mathscr{V}}{5N}\left(\eta^0_{eff} - \eta\right)\left[\frac{1}{2}\overline{\boldsymbol{rot}\,\boldsymbol{V_0}}|_z - \langle\omega_z\rangle\right], \tag{5.5}$$

where we have replaced $5/2\phi\eta$ by $(\eta^0_{eff} - \eta)$. This is exact for dilute regimes and empirical for more concentrated regimes. The term $\overline{\boldsymbol{rot}\,\boldsymbol{V_0}}|_z$ is the z-component of the vorticity averaged on the total volume of the suspension in the absence of torque (Ichiki & Prosperetti 2004). But since we impose a given shear rate, we get $\overline{\boldsymbol{rot}\,\boldsymbol{V_0}}|_z = -\dot\gamma$. Thus we can write

$$L = \frac{12\mathscr{V}}{5N}\left(\eta^0_{eff} - \eta\right)\left(\frac{\dot\gamma}{2} + \langle\omega_z\rangle\right). \tag{5.6}$$

In our simulations, for a given volume fraction we impose the same value of the torque L on each particle and we calculate the value of ω_z averaged on all the particles. This is shown in figure 14. The numerical results are indeed very well fitted with (5.6). Yeo & Maxey (2010) plotted η_{eff} as a function of a non-dimensional value of the torque $L^* = L/(8\pi\eta R^3\dot\gamma)$. Here, we plot their values as a function of Θ to show that their data are very well fitted by (5.3). Note that from (5.6) we obtain the following relation between L^* and Θ:

$$L^* = \frac{\Delta\eta^0_{eff}(\phi)}{5\phi}\Theta. \tag{5.7}$$

For dilute regimes ($\phi \ll 1$), we have $L^* = \Theta/2$, but for higher values of ϕ the relationship (5.7) between the two dimensionless numbers depends nonlinearly on ϕ. For example, when $\phi = 40\,\%$, (5.7) gives $L^* \approx 2.0\,\Theta$.

Figure 15 shows the critical values of the torque per particle $L^*_c = L_c/(8\pi\eta R^3\dot\gamma)$ needed to obtain $\Theta = -5/3$ (i.e. $\Delta\eta_{eff} = 0$). When $\phi \ll 1$, L_c tends to a constant value independent of ϕ, $L_c = (20/3)\pi R^3\eta\dot\gamma$ (i.e. $L^*_c = -5/6$), it is the torque per particle that is needed to obtain $\Theta = -5/3$ in the dilute regime.

Equation (5.6) could be generalized in the following vectorial equation:

$$\boldsymbol{L} = -\frac{12\mathscr{V}}{5N}(\eta^0_{eff} - \eta)\left[\frac{1}{2}\overline{\boldsymbol{rot}\,\boldsymbol{V_0}} - \langle\boldsymbol{\omega}\rangle\right]. \tag{5.8}$$

Note that expression (5.8) tends to the usual Faxén law (3.1) for dilute regimes, i.e. when $\phi \ll 1$.

https://doi.org/10.1017/jfm.2011.535 Published online by Cambridge University Press

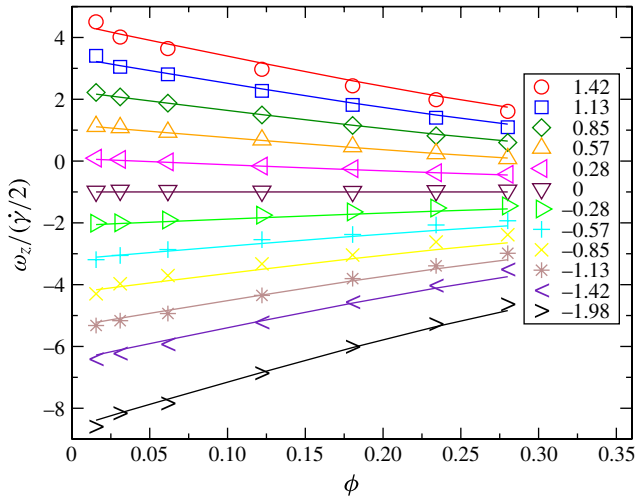


FIGURE 14. (Colour online) The dimensionless angular velocity as a function of volume fraction for several values of the applied dimensionless torque $L^* = L/(8\pi R^3\eta\dot\gamma)$.

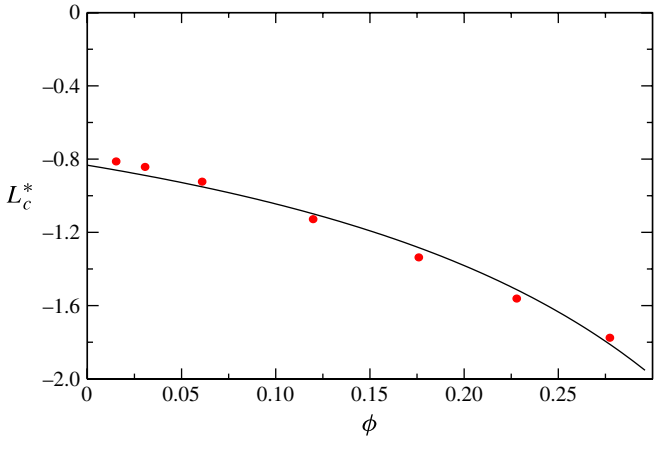


FIGURE 15. (Colour online) The values of the dimensionless torque $L_c^* = L_c/(8\pi R^3\eta\dot\gamma)$ as a function of ϕ for which $\Theta = -5/3$ (i.e. $\Delta\eta_{eff} = 0$). Circles, numerical data; solid curve, (5.6) with $\langle\omega_z\rangle = -4/3\dot\gamma$, i.e. $\Theta = -5/3$. Note that L_c^* tends to $-5/6$ for $\phi \ll 1$.

We can recover the expression (5.3) of the relative effective viscosity in the presence of a torque for high concentrations. The xy-stress is given by

$$\sigma_{xy}^R = \frac{N L_z}{2\mathscr{V}} = \frac{6}{5}(\eta_{eff}^0 - \eta)\langle\Omega\rangle, \tag{5.9}$$

and, using $\eta_{eff} = \eta_{eff}^0 + \eta_{eff}^R$ with $\eta_{eff}^R = \sigma_{xy}^R/\dot\gamma$, we obtain

$$\eta_{eff} = \eta_{eff}^0 + \frac{3}{5}(\eta_{eff}^0 - \eta)\frac{\langle\Omega\rangle}{\dot\gamma/2}, \tag{5.10}$$

which is equivalent to the expression (5.3).

https://doi.org/10.1017/jfm.2011.535 Published online by Cambridge University Press

6. Conclusions

In this paper, we show that we can tune the effective viscosity of a sheared suspension of neutrally buoyant spherical particles if they are sensitive to an external torque that modifies their rotation. The competition between the two effects (shear flow and torque) is well described by the dimensionless number Θ, representing the relative angular velocity of the particles divided by the vorticity of the shear flow. Enhancement and reduction of the shear-effective viscosity are found, and depend on the applied torque intensity and sign. For a given value of the mean angular velocity of the particles ($\langle\omega_z\rangle = -4/3\dot{\gamma}$), which is independent of the volume fraction, the contribution of the particles to the effective viscosity can be suppressed and the effective viscosity of the suspension becomes equal to the viscosity of the solvent. An empirical formula is proposed for the effective viscosity of the suspension, which fits the data remarkably well. We can recover this law by using an empirical form of Faxén's second law adapted to a more concentrated regime (up to 40 %).

Acknowledgements

We would like to acknowledge the useful comments of C. Misbah and C. Verdier as well as the financial support from ANR grant MOSICOB and from the Region Rhône-Alpes via the CIBLE program.

REFERENCES

BACRI, J. C., PERZYNSKI, R., SHLIOMIS, M. I. & BURDE, G. 1995 Negative-viscosity effect in a magnetic fluid. *Phys. Rev. Lett.* **75**, 2128–2131.

BARTOK, W. & MASON, S. G. 1957 Particle motions in sheared suspensions. *J. Colloid Sci.* **12**, 243–262.

BATCHELOR, G. K. 1970 The stress system in a suspension of force-free particles. *J. Fluid Mech.* **41**, 545–570.

BATCHELOR, G. K. & GREEN, J. T. 1972 The determination of the bulk stress in a suspension of spherical particles to order c^2. *J. Fluid Mech.* **56**, 401–427.

BRADY, J. F., PHILIPS, R. J., LESTER, J. C. & BOSSIS, G. 1988 Dynamic simulation of hydrodynamically interacting suspensions. *J. Fluid Mech.* **195**, 257–280.

BRENNER, H. 1970 Rheology of a dilute suspension of dipolar spherical particles in an external field. *J. Colloid Interface Sci.* **32**, 141–158.

CICHOCKI, B. & FELDERHOF, B. U. 1988 Short-time diffusion coefficients and high frequency viscosity of dilute suspensions of spherical Brownian particles. *J. Chem. Phys.* **89**, 1049–1054.

CONDIFF, D. W. & DAHLER, J. S. 1964 Fluid mechanical aspects of antisymmetric stress. *Phys. Fluids* **7**, 842–854.

DA CUNHA, F. R. & HINCH, E. J. 1996 Shear-induced dispersion in a dilute suspension of rough spheres. *J. Fluid Mech.* **309**, 211–223.

DAVIT, Y. & PEYLA, P. 2008 Intriguing viscosity effects in confined suspensions: a numerical study. *Eur. Phys. Lett.* **83**, 64001.

EINSTEIN, A. 1906 Eine neue Bestimmung der Moleküldimensionen. *Ann. Phys. (Leipzig)* **19**, 289–306.

EINSTEIN, A. 1911 Berichtigung zu meiner Arbeit: 'Eine neue Bestimmung der Moleküldimensionen'. *Ann. Phys. (Leipzig)* **34**, 591–592.

FENG, S., GRAHAM, A. L., ABBOTT, J. R. & BRENNER, H. 2006 Antisymmetric stresses in suspensions: vortex viscosity and energy dissipation. *J. Fluid Mech.* **563**, 97–122.

GADALA-MARIA, F. 1979 The rheology of concentrated suspensions. PhD thesis, Stanford University.

HAPPEL, J. & BRENNER, H. 1983 *Low Reynolds Number Hydrodynamics*. Martinus Nijhoff.

ICHIKI, K. & PROSPERETTI, A. 2004 Faxen-like relations for a non-uniform suspension. *Phys. Fluids* **16**, 2483–2496.

https://doi.org/10.1017/jfm.2011.535 Published online by Cambridge University Press

ISHIKAWA, T. & PEDLEY, T. J. 2007 The rheology of a semi-dilute suspension of swimming model micro-organisms. *J. Fluid Mech.* **588**, 399–435.

JEFFERY, G. B. 1922 The motion of ellipsoidal particles immersed in a viscous fluid. *Proc. R. Soc. Lond.* **102**, 161–179.

KRIEGER, I. M. & DOUGHERTY, T. J. 1959 A mechanism for non-Newtonian flow in suspensions of rigid spheres. *Trans. Soc. Rheol.* **3**, 137–152.

KROMKAMP, J., VAN DEN ENDE, D., KANDHAI, D., VAN DER SMAN, R. & BOOM, R. 2006 Lattice Boltzmann simulation of 2D and 3D non-Brownian suspensions in Couette flow. *Chem. Engng Sci.* **61**, 858–873.

LADD, A. J. C. 1990 Hydrodynamic transport coefficients of random dispersions of hard spheres. *J. Chem. Phys.* **93**, 3484–3494.

LANDAU, L. & LIFSCHITZ, E. 1959 *Fluid Mechanics*. Pergamon.

LEMAIRE, E., LOBRY, L. N., PANNACCI, F. & PETERS, 2008 Viscosity of an electro-rheological suspension with internal rotations. *J. Rheol.* **52**, 769–785.

LIM, S., PARK, S. M. & KIM, K. I. 2005 AI vibration control of high-speed rotor systems using electrorheological fluid. *J. Sound Vib.* **284**, 685–703.

MARCHIORO, M., TANKSLEY, M. & PROSPERETTI, A. 2000 Flow of spatially non-uniform suspensions. Part I. Phenomenology. *Intl J. Multiphase Flow* **26**, 783–831.

MARCHIORO, M., TANKSLEY, M., WANG, M. & PROSPERETTI, A. 2001 Flow of spatially non-uniform suspensions. Part II. Systematic derivation of closure relations. *Intl J. Multiphase Flow* **27**, 237–276.

MARSHALL, L., ZUKOVSKI, C. F. & GOODWIN, J. W. 1989 Effects of electric fields on the rheology of non-aqueous concentrated suspensions. *J. Chem. Soc. Faraday Trans.* **85**, 2785–2795.

MAURY, B. 2006 A time stepping scheme for inelastic collisions. *Numer. Math.* **102**, 649–679.

MAURY, B. 2009 Numerical analysis of a finite element/volume penalty method. *SIAM J. Numer. Anal.* **47**, 1126–1148.

MIKULENCAK, D. R. & MORRIS, J. F. 2004 Stationary shear flow around fixed and free bodies at finite Reynolds number. *J. Fluid Mech.* **520**, 215–242.

PEYLA, P. 2007 Rheology and dynamics of a deformable object in a microfluidic configuration: a numerical study. *Eur. Phys. Lett.* **80**, 34001.

PEYLA, P. & VERDIER, C. 2011 New confinement effects on the viscosity of suspensions. *Eur. Phys. Lett.* **94**, 44001.

PEYRET, R. & TAYLOR, T. D. 1963 *Computational Methods for Fluid Flow*. Springer.

PHANI, A. S. & VENKATRAMAN, K. 2005 Damping characteristics of electro-rheological fluid sandwich beams. *Acta. Mechanica* **180**, 195–201.

RAFAÏ, S., JIBUTI, L. & PEYLA, P. 2010 Effective viscosity of microswimmer suspensions. *Phys. Rev. Lett.* **104**, 098102.

ROSENSWEIG, R. E., KAISER, R. & MISKOLCZY, C. 1969 Viscosity of magnetic fluid in a magnetic field. *J. Colloid Interface Sci.* **29**, 680–686.

RUSSEL, W. B., SAVILLE, D. A. & SCHOWALTER, W. R. 1989 *Colloidal Dispersions*. Cambridge University Press.

SIEROU, A. & BRADY, J. F. 2002 Rheology and microstructure in concentrated noncolloidal suspensions. *J. Rheol.* **46**, 1031–1056.

TAN, K. P., STANWAY, R. & BULLOUGH, W. A. 2006 Dynamic velocity response of an electro-rheological (ER) clutch for robotic applications. *Mech. Adv. Mater. Struct.* **13**, 1–12.

TANAKA, H. & ARAKI, T. 2000 Simulation method of colloidal suspensions with hydrodynamic interactions: fluid particle dynamics. *Phys. Rev. Lett.* **85**, 1338–1341.

THOMAS, D. G. 1969 Transport characteristics of suspensions. Part VIII. A note on the viscosity of Newtonian suspensions of uniform spherical particles. *J. Colloid Sci.* **20**, 267–277.

WANG, W. & PROSPERETTI, A. 2001 Flow of spatially non-uniform suspensions. Part III. Closure relations for porous media and spinning particles. *Intl J. Multiphase Flow* **27**, 1627–1653.

YEO, K. & MAXEY, M. R. 2010 Rheology and ordering transitions of non-Brownian suspensions in a confined shear flow: effects of external torques. *Phys. Rev.* E **81**, 062501.

https://doi.org/10.1017/jfm.2011.535 Published online by Cambridge University Press